DERIVING LUNAR MINERAL ABUNDANCE MAPS FROM CLEMENTINE MULTISPECTRAL IMAGERY. L. Li[1] and S. Li[1], [1]Department of Earth Sciences, 723 W. Michigan Street, Indiana University-Purdue University, Indianapolis, IN, 46202; emails: ll3@iupui.edu and shuali@imail.iu.edu.

Introduction: Global maps of lunar geochemistry and mineralogy have a number of applications in examining the magma ocean hypothesis on the origin and evolution of lunar crust and mantle structures, getting insight into the characteristic of lunar mantle, investigating basaltic volcanism, impact crater/basin structures and ejecta emplacement, and lunar soil evolution and mixing mechanisms, and planning future lunar missions (e.g. landing site selection).

Commonly used methods for estimating the abundance of lunar soil minerals and chemicals from laboratory or remotely measured spectral reflectance include empirical methods using spectral parameters [1-3], multivariate statistical analysis [4-9], the Modified Gaussian Model (MGM) [10] and radiative transfer modeling [11-13]. The use of empirical methods has been focused on mapping lunar soil FeO and TiO2; the MGM requires well defined spectral absorption bands that are represented well by hyperspectral data and radiative transfer modeling is computational expensive when applied to high spatial resolution hyper- and multi-spectral images. In contrast, multivariate statistical analysis has the capability of mapping lunar soil mineralogy with either hyperspectral or multispectral images in a timely efficient manner. Here we introduce an approach to mapping major lunar minerals with Clementine ultraviolet (UV), visible (VIS) and near infrared (NIR) multispectral images, in which genetic algorithms (GA) and partial least squares (PLS) regression are jointly used. The effectiveness of GA-PLS was demonstrated with the Clementine UV-VIS-NIR image of a lunar region including Mare Serenitatis, Mare Transquillitatis, Mare Crisium and Mare Nectaris and thus showing a variety of different mare soils.

Methods: Clementine UV-VIS-NIR data at 1 km spatial resolution were used to generate the mineral maps of the example area. While Clementine NIR data have six spectral bands centered at 1.1, 1.25, 1.5, 2.0, 2.6, 2.78 μm, the first four bands of the Clementine NIR dataset were analyzed together with the Clementine UVVIS data considering the effect of thermal emission on the last two NIR bands.

Unlike hyperspectral data (e.g. M3), multispectral data have a limited number of spectral bands and lack detailed spectrally diagnostic characteristics. To overcome this limitation, we used Clementine UV-VIS-NIR spectral band ratios and curvatures as additional input variables for the GA-PLS model together with the original spectral bands. Some of band ratios are "key ratio" related to mafic mineral abundances, while "spectral curvature" is linked to absorption band shape which can be distinguished between low- and high-Ca pyroxene and olivine [14]. In previous studies [4-6], only predetermined ratios and curvatures were used; here the potential of all possible, distinct band ratios (i.e., the Clementine 0.415/0.750 μm ratio is not distinctive from the ratio of 0.750/0.415 μm) and band curvatures as additional spectral variables for mapping lunar soil composition were examined.

A simple PLS model consists of two outer relations and one inner relation. The two outer relations result from eigenstructure decompositions of both the matrix containing explanatory variables (i. e., spectral bands) and the matrix containing response variables (i. e., lunar mineral abundance), while the inner relation links the resultant score matrices from the two eigenstructure decompositions generating the outer relations [15]. Let both X [$n\times m$] represent a explanatory matrix, the first outer relation is derived by applying principal component analysis (PCA) to X, resulting in the score matrix T [$n\times a$] and the loading matrix P' [$a\times m$] plus an error matrix E [$n\times m$], i.e. $X = TP' + E$ Similarly, the second outer relation for Y [$n\times p$] standing for a response variable matrix can be derived by decomposing Y into the score matrix U [$n\times a$] and the loading matrix Q' [$a\times p$] and the error term F [$n\times p$], i.e. $Y = UQ' + F$. The prime represents matrix transpose. The inner relation $U = BT$ is a multiple linear regression between the score matrices U and T in which B is an $n\times n$ regression coefficient matrix determined via least square minimization. The goal of the PLS model is to minimize the norm of F while maximizing the covariance between X and Y by the inner relation. Because the above-mentioned two separate PCAs' approach to deviating PLS factors is not the best possible and results in a weak correlation for the inner relation, a method resulting in a strong inner relation between T and U was used [9, 15].

Genetic algorithms (GA) are a computer model that simulates natural selection [16]. A genetic algorithm includes at least five components: encoding, population initialization, individual selection, crossover and mutation [16]. For encoding a genetic algorithm works with a population of randomly generated chromosomes (i.e. candidate solution) in population initialization, and each chromosome is formed by as many “bits” as the number of spectral bands, and “zeros’ or “ones” are assigned to the bits of that chromosome. A zero bit indicates the band is not selected and an one bit means otherwise. Crossover is the process of reproducing

new offspring by exchanging genes between two reproducing chromosomes, and then mutation follows and simulates the gene change of a chromosome due to the random disturbance. Because GA is well suitable for generating a subset of spectral bands and removing spectral bands that are insensitive to response variables [17].

We used the LSCC data resampled into the Clementine UV-VIS-NIR spectral resolution to build the spectral-mineral models, in which 57 LSCC samples from particle size groups: 45-20, 20-10, <10 μm were used in calibration.

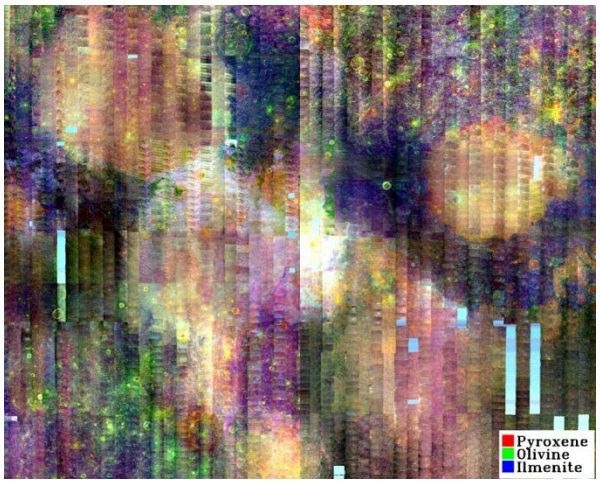

Figure 1. A map shows the abundance of pyro.(R), oliv.(G) and ilmen.(B) in the region including Mare Serenitatis, Mare Tranquillitatis, Mare Crisium, Mare Fecunditatis and Mare Nectaris.

Results and Discussion: GA-PLS resulted in a high coefficient of determination for agglutinate (R^2= 0.63), pyroxene (R^2= 0.81), plagioclase (R^2= 0.85), ilmenite (R^2= 0.72), olivine (R^2= 0.48), but a low correlation for volcanic glass (R^2= 0.39). These results are consistent with those reported in our previous work [7]. Poor correlations for olivine and volcanic glass may stem from a narrow range of their abundances and the fact that the LSCC samples are not representative. The calibrated GA-PLS models were applied to the Clementine UV-VIS-NIR of the example area for producing the mineral maps of this area and a color composite image showing pyroxene as red, olivine as green and ilmenite as blue is presented in Figure 1.

While Figure 1 shows significant amounts of noise due to mosaic lines in horizontal and vertical directions, the map still reflects the differences in compositional pattern among these maria and within a single mare. For example, Mare Tranquillitatis shows more olivine and ilmenite than Mare Crisium, and Mare Serenitatis shows the lowest olivine and ilmenite. High olivine and ilmenite areas also include the Apollo 17 landing area and part of Mare Tranquillitatis close to the boundary between itself and Mare Serenitatis.

However, caution must be taken to explain the color pattern in the highland region around these maria and highland contaminated maria. For example, Mare Fecunditatis shows a high amount of ilmenite, which seems higher than Mare Serenitatis and reaches the same level as that of Mare Transquillitatis. This compositional pattern may not be true in reality. Examining the correlation between measured and modeled ilmenite abundances indicated that the model yielded large errors when modeling very low-Ti and low-Ti mare and highland samples because of overestimation. This is why highland regions around the maria show blue or purple colors. This is due to the highland contamination caused by Langrenus so that Mare Fecunditatis seems to have a high amount of ilmenite. The reason also explains the purple color of Mare Nectaris.

Conclusions: Application of GA-PLS does show some success in mapping lunar major minerals as demonstrated by high coefficients of determination and the mineral maps of the example area (Figure 1). Two issues to be addressed in the further work are: 1) the type of noise shown in Figure 1 needs to be compensated and 2) the correlations for olivine and volcanic glass need to be improved. Minimum noise transform (MNF) or band modeling/fitting being conducted before GA-PLS modeling could be two optional procedures for removing the noise. Additional calibration spectra are needed to improve the prediction of olivine, volcanic glass and ilmenite in low-Ti samples. We propose to use the Hapke's forward model to expand the range of the LSCC sample so that olivine-rich basalts, and magnesian highland samples (e.g. troctolites) are included in the GA-PLS calibration dataset [18]. The GA-PLS method can be easily adapted for mapping the mineralogy of a planetary body with hyperspectral images acquired by the current and future missions to the Moon and Mercury.

References: [1] Lucey P. G. et al. (1998) *JGR*, 103, 3701-3708. [2] Lucey P. G. et al. (1998) *JGR*, 103, 3679-3699. [3] Lucey P. G. et al. (2000) *JGR*, 105, 20,297-20,305. [4] Shkuratov Y. G. et al. (2005) *Solar Sys. Res.*, 39(4), 255-266. [5] Pieters C. M. et al. (2002) *Icarus*, 155, 285-298. [6] Pieters C. M. et al. (2006) *Icarus*,184,83-101. [7] Li L. (2006) *JGR*, doi:10.1029/2005JE002598. [8] Li L. (2008) *Adva. in Space Res.*, 42(2):267-274. [9] Li L. (2008) JGR, 113, E12013, doi:10.1029/2008JE003213. [10] Sunshine J. M. and Pieters C. M. (1993) *JGR*, 98, 9075–9087. [11] Lucey P. G. (2006) JGR, doi:10.1029/2005JE002661. [12] Lucey P. G. (2004) *Geophys. Res. Lett.*, doi:10.1029/2003GL019406. [13] Lawrence S. J. and Lucey P. G. (2007) *JGR*, doi:10.1029/2006JE002765. [14] Tompkins S. and Pieters C. M. (1999) *Metero. and Planet. Sci.*, 3, 25-41. [15] Geladi P. and Kowalski B. (1986) *Analy. Chimi. Acta*, 185, 1-17. [16] Forrest S. (1993) *Science*, 261, 872-878. [17] Li et al. (2007) *IEEE Trans. Geosci. and Remote Sens. Lett.*, 4(2), 216-220. [18] Li S. and Li L. (2009) *LPSC XXXXI*, abstract # 2168.